J Solid State Electrochem (2012) 16:2717–2722
DOI 10.1007/s10008-012-1660-4

ORIGINAL PAPER

Comparison of carbon aerogel and carbide-derived carbon as electrode materials for non-aqueous supercapacitors with high performance

Ann Laheäär · Anna-Liisa Peikolainen · Mihkel Koel · Alar Jänes · Enn Lust

Received: 22 November 2011 / Revised: 11 January 2012 / Accepted: 14 January 2012 / Published online: 1 March 2012

Abstract Two porous carbon materials, one synthesised by pyrolysis of an organic aerogel prepared using sol–gel method and the other synthesised from molybdenum carbide by high temperature chlorination method, were tested as supercapacitor electrode materials in a non-aqueous tetraalkylammonium salt-based electrolyte. The gravimetric capacitance values calculated for the carbon aerogel (CAG)-based system were almost two times smaller (~55 Fg^{-1}) compared to carbide-derived carbon ($C(Mo_2C)$)-based system (~125 Fg^{-1}). However, due to the very wide region of ideal polarizability, 3.6 V for $C(Mo_2C)$ and 3.8 V for CAG-based test cells, very high energy densities up to 63 Wh kg^{-1} (34 Wh dm^{-3}) and power densities up to 757 kW kg^{-1} (314 kW dm^{-3}) were estimated for these systems, respectively. CAG-based system shows very short characteristic charge/discharge time constant values (0.05 s).

Keywords Supercapacitor · Carbide-derived carbon · Carbon aerogel · Non-aqueous electrolyte

A. Laheäär · A. Jänes · E. Lust (✉)
Institute of Chemistry, University of Tartu,
Ravila 14a,
50411 Tartu, Estonia
e-mail: enn.lust@ut.ee

A.-L. Peikolainen · M. Koel
Department of Chemistry, Tallinn University of Technology,
Akadeemia Tee 15,
12618 Tallinn, Estonia

Introduction

Recently, renewable energy sources, such as solar power and wind energy, have been under quick development. However, these energy sources are erratic and their attainability depends noticeably on the time of day and season. Consequently, energy storage systems are needed to widely utilise these renewable energy sources, including their connection with smart grids. Among different energy storage systems, the electrochemical power sources (Li-ion batteries, supercapacitors and fuel cells) are highly valued choices [1–10] that can easily be produced in the form of both small and large capacity devices.

During the last few decades, intensive research and development work has been done in the field of supercapacitors (SCs) with the aim to improve the energy and power performance of these energy storage devices [1–6]. Many different porous carbon materials have been studied as potential electrode materials in both aqueous and non-aqueous electrolyte-based capacitor systems [7, 8]. It was established that limiting capacitance and characteristic time constant [3–8], and thus, energy and power density, depend noticeably on the specific surface area and pore size distribution of the carbon materials studied. This paper focuses on the comparison of electrochemical behaviour of two different carbon materials for non-aqueous electrolyte-based SC application—mainly microporous high surface area carbide-derived carbon (with some mesoporosity) and partly mesoporous carbon aerogel with a small contribution of very narrow micropores.

Carbon aerogels, prepared by different synthesis methods, have been studied as porous SC electrodes [11], also as composite electrode materials [12] and conductive fillers for activated carbon-based electrodes [13]. The electrochemical

behaviour of different carbide-derived carbons as electrode materials has also been tested [14, 15].

Experimental

Electrode active material synthesis, porosity and X-ray diffraction characterization

Carbon aerogel material, further noted as CAG, was synthesised from a gel of 5-methylresorcinol (MR) (99.6%, Carboshale OÜ) and formaldehyde (FA) (37% aqueous solution (Sigma-Aldrich) stabilised with 10–15% of methanol). The initial gel was prepared at 25 °C by dissolving MR and Na_2CO_3 (99.8%, Riedel-de Haën) in deionized water (W), followed by the addition of FA solution. Concentrations of the precursors, expressed as molar ratios, were the following: MR/FA=0.5, W/MR=45 and MR/Na_2CO_3=60. Twenty-four hour after gel formation, the gel monolith was placed into aqueous acetic acid (≥99%, Sigma-Aldrich) solution (pH≈4) for 48 h to neutralise the base catalyst in the gel. Solvent exchange in the gel pores was done by placing the gel into acetone (≥99.5%, BaltOil AS, replaced every 24 h for 4 days with the volume of acetone being ten times the volume of gel piece). Then, the gel was dried via supercritical carbon dioxide extraction on a 100-ml autoclave (constructed by NWA Analytische Meßgeräte GmbH) to obtain an organic aerogel. Carbon aerogel was prepared by heating the organic aerogel up to 900 °C in a nitrogen flow, following a temperature programme proposed by Pérez-Caballero et al. [16]. Activation of the carbon aerogel was carried out in a CO_2 flow at 900 °C for 2 h with the temperature ramping rate 10 °C min^{-1}. A tubular furnace MTF 12/38/400 (Carbolite) was applied for carbonization and activation. High temperature chlorination method, described in detail in Ref. [17], was used at 800 °C for synthesising mainly microporous carbide-derived carbon from molybdenum carbide, noted as C(Mo_2C).

Nova 1200e (Quantachrome) system was used for nitrogen adsorption measurements, where Brunauer–Emmett–Teller method, non-local density functional theory (NLDFT) and other models, discussed in detail in [18], were applied to study the porous carbon structure. Slit-shaped pores were assumed and a standardised model was applied for the N_2 sorption data analysis by NLDFT [19]. The data obtained for C(Mo_2C) and CAG are given in Table 1 and pore size distributions are represented in Fig. 1a. According to the adsorption measurements, C(Mo_2C)-based electrode material, having one NLDFT pore size distribution maximum (PSDM) at 1.15 nm, is mainly microporous with some mesoporosity with second PSDM at 3.80 nm. CAG has a considerable amount of both mesopores and micropores, but the micropores are much smaller compared to C(Mo_2C), having the respective PSDM at ~0.55 nm (Fig. 1a), and probably contribute little to the overall actively adsorbing pore volume of CAG material (Table 1). Thus, for CAG material, mesopores form most of the active surface for adsorption of electrolyte ions.

Table 1 Gas phase characteristics of the C(Mo_2C) and CAG electrode materials

Carbon	S_{BET}/m^2 g^{-1}	S_{micro}/m^2 g^{-1}	V_{micro}/cm^3 g^{-1}	V_{tot}/cm^3 g^{-1}
C(Mo_2C)	1,680	1,560	1.2	1.4
CAG	790	440	0.2	2.2

BET Brunauer–Emmett–Teller, S_{BET} BET multipoint surface area, S_{micro} *t*-method micropore area, V_{micro} *t*-method micropore volume, V_{tot} total pore volume

The X-ray diffraction (XRD) pattern for the CAG electrode material (Fig. 1b) was recorded on a Bruker D8 diffractometer (Bruker Corp.) employing CuKα radiation with a step size of 0.01° and counting time of 2 s using position sensitive LynxEye detector. The diffraction spectrum was recorded at 25 °C. Similar XRD profiles have been obtained for carbon aerogel materials synthesised by other

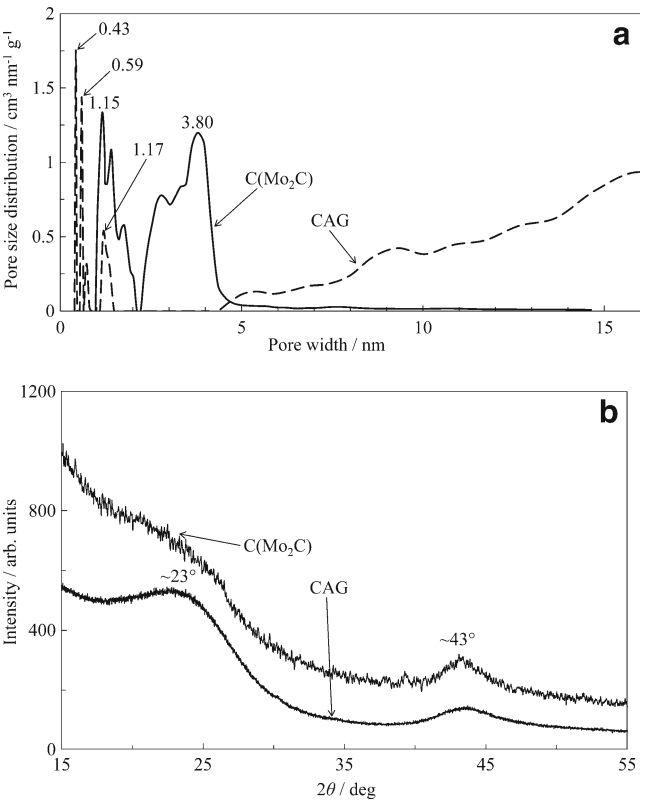

Fig. 1 **a** Differential pore size distribution vs. pore width plots obtained by applying NLDFT method on the nitrogen sorption (at −196 °C) data and **b** characteristic XRD patterns for CAG and C(Mo_2C) electrode materials

research groups [20, 21]. The XRD pattern for C(Mo_2C) material has been published before [17] and is reproduced for comparison in Fig. 1b. According to data in Fig. 1b, both CAG and C(Mo_2C) are practically amorphous. However, there is a small amount of graphitic structure in both materials based on the wide diffraction peaks at 2θ~23° and 2θ~43°, characteristic to the graphite (002) and (100)/(101) planes, respectively [17]. The (002) diffraction peak corresponds to parallel graphene layers and (100)/(101) diffraction peak describes the 2D in-plane symmetry along the graphene layers. More detailed C(Mo_2C) material characterization can be found in [17].

Experimental systems

The 105±5-μm thick layers of electrodes were press-rolled from slurries comprising 95 wt.% active material, C(Mo_2C) or CAG and 5 wt.% polytetrafluoroethylene (PTFE) binder (required amount of PTFE measured from 60% solution in H_2O (Aldrich)). A thin Al layer (~2 μm) was deposited by magnetron sputtering method (AJA International) on one side of the electrodes for good electrical contact and to reduce the ohmic potential drop for SC cells. Cross-section surface area of electrodes in the assembled symmetrical two-electrode test cells was 2.0 cm^2. The mass per two electrodes was ~0.018 and ~0.023 g for CAG- and C(Mo_2C)-based systems, respectively.

The SC systems were tested in 1 M triethylmethylammonium tetrafluoroborate ($TEMABF_4$, 99.9%, Stella Chemifa Corp.) solution in acetonitrile (AN, 99.9%, max 0.003% H_2O, Riedel-de Haën). The electrolyte solution was saturated with pure Ar (99.9999%) and all measurements were conducted in a glove box using hermetic two-electrode standard cells (Hohsen Corp.). Membranes made from cellulose (TF4425, Nippon Kodoshi Corp.) were used for optimal chemical compatibility with AN-based electrolyte. Electrodes were impregnated with the working electrolyte solution for 24 h before measurements. Impedance spectra were recorded using a 1252A Solartron frequency response analyser and a SI1287 potentiostat with a 5-mV modulation.

Electrochemical results and discussion

Cyclic voltammetry data

The cyclic voltammograms (CVs) were measured at cell potential scan rates ν from 5 to 100 mV s^{-1} up to different maximum cell potentials ΔE to establish regions of ideal polarizability for each porous carbon electrode material. The gravimetric capacitance C_g (in farads per gram) and volumetric capacitance C_v (in farads per centimetre) values per one electrode were calculated from the current density j (in amperes per square centimetre) values on CVs according to:

$$C_g = \frac{2j \times S_{el}}{\nu \times m_{el}} \quad (1)$$

$$C_v = \frac{2j}{\nu \times l_{el}} \quad (2)$$

where ν is cell potential scan rate (in volts per second), S_{el} is electrode cross-section surface area (2.0 cm^2), m_{el} is mass per one electrode (in grams) and l_{el} is electrode thickness (105 μm).

According to CV data (expressed as C_g vs. ΔE) in Fig. 2a, ΔE as high as 3.8 V can be applied in a symmetrical system with CAG electrodes and 1 M $TEMABF_4$ electrolyte in AN. A fairly rectangular shape of CVs is maintained even at such high ΔE with the start of some faradaic electrolyte solvent/salt decomposition reaction or oxidation/reduction of surface functionalities on the CAG surface near ΔE=3.8 V. There is no distortion in the shape of CVs even at high cell potential scan rate (100 mV s^{-1}), which indicates relatively fast adsorption/desorption processes in this system, explainable by the fast diffusion of ions in the mesoporous CAG

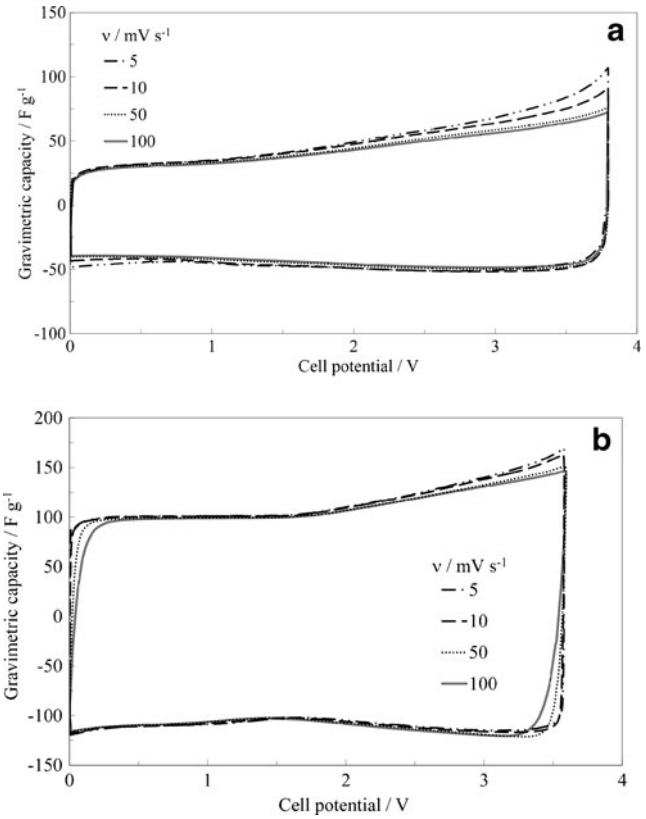

Fig. 2 CVs, presented as gravimetric capacitance vs. cell potential, for **a** CAG- and **b** C(Mo_2C)-based SC test cells at different cell potential scan rates ν, given in the figure

structure. Taking into consideration the very narrow micropores on the CAG electrode surface, (partial) solvation shell removal has to occur for the diffusion of electrolyte ions into these pores ($TEMA^+$ ions may be too large to diffuse in micropores even with partial solvation shell) [1, 5, 6, 14, 15]. Thus, the slightly smaller C_g values obtained at lower ΔE applied ($\Delta E<2$ V) are probably explainable by inefficient solvation shell removal due to weaker electrostatic attraction forces in this region and higher effective Debye length values at lower electrode potentials [5, 14, 22].

The CVs for a test system with $C(Mo_2C)$ electrodes (Fig. 2b) in 1 M $TEMABF_4$ + AN electrolyte have nearly rectangular shape up to $\Delta E=3.6$ V. The calculated C_g values are more than two times higher compared to the CAG-based system. This can be explained by the approximately two times higher specific surface area of the $C(Mo_2C)$ material (Table 1) and also by the prevalence of somewhat larger micropores (Fig. 1a) that are more easily accessible for the large $TEMA^+$ cations and also for BF_4^- anions. There is a small distortion in the shape of CVs at $\nu=100$ mV s^{-1} caused by slower diffusion processes [4, 5, 17] in the practically microporous carbon structure compared to the partially mesoporous structure of CAG. The calculated C_v values for the $C(Mo_2C)$- and CAG-based systems were high (~70 F cm^{-3}) and moderate (~20 F cm^{-3}), respectively.

Impedance spectroscopy data

The Nyquist plots (Z'' vs. Z') were measured in a frequency range from 1×10^{-3} to 3×10^{5} Hz at different ΔE applied. The Nyquist plots for both systems studied showed nearly ideal capacitive behaviour in the low-frequency part (Fig. 3a, b), where the rate-limiting step is adsorption on the micro-/mesoporous surface of electrodes [5, 6]. The plots obtained for $C(Mo_2C)$-based test cells were slightly more vertical (more pronounced ideal capacitive behaviour) at low frequencies, and there is a well-defined 'porous electrode section' in the middle-frequency region with a −45° slope (Fig. 3b, inset), where diffusion-like mass transfer process is the rate-limiting step [5, 6, 14, 22]. For CAG-based system, the slope in middle-frequency region is less than −45° (Fig. 3a, inset), which means that mixed kinetic processes are taking place (charge transfer on macroscopic electrode surface, diffusion in porous structure and adsorption mainly on mesopores) [6]. The high-frequency equivalent series resistance (R_E) values obtained for CAG-based system were slightly smaller (~0.6 Ω cm^2) compared to $C(Mo_2C)$-based system (~0.8 Ω cm^2), demonstrating the better electrical conductivity of CAG electrodes as well as higher electrolyte conductivity in mesopores of CAG structure.

The phase angle θ vs. frequency f plots (Fig. 4) reach −87° and −89° in the low-frequency region in systems with

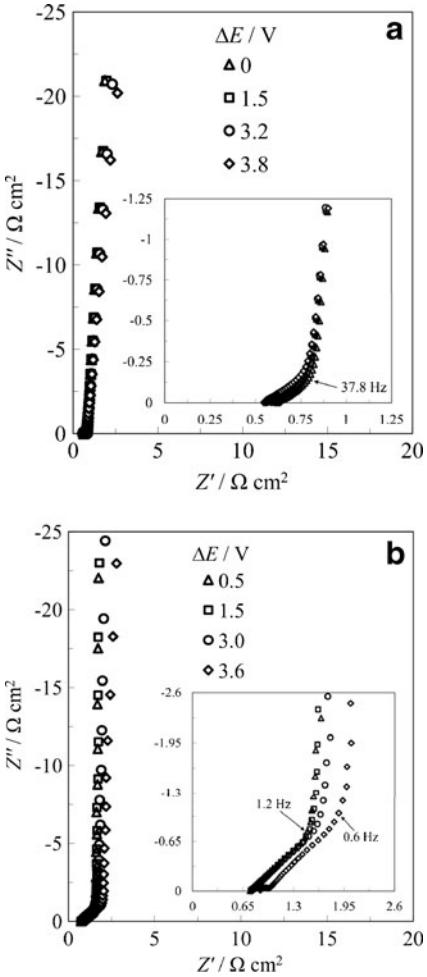

Fig. 3 Impedance spectra for **a** CAG- and **b** $C(Mo_2C)$-based SC test cells at different cell potentials ΔE applied, given in the figure

CAG and $C(Mo_2C)$ electrodes, respectively, indicating that both systems studied have nearly ideally capacitive behaviour. However, the capacitive plateau is reached at higher frequencies in the system with CAG electrode due to the higher mesopore volume in comparison with $C(Mo_2C)$, which means that CAG system has a shorter characteristic time constant (discussed later in this paper). There is a small decrease in the $|\theta|$ values at higher ΔE applied ($\Delta E\geq3.4$ V) in the low-frequency region ($f<3$ mHz) indicating the beginning of some slow faradaic reactions at the surfaces both electrodes (electrolyte decomposition, oxidation/reduction of surface functionalities and electrochemical reaction of H_2O and O_2 traces).

Time constants and energy/power density calculations

The characteristic charge/discharge time constants τ_R, showing how much time it takes to release half of the maximal energy stored in the SC, were calculated from the frequencies of maxima f_{max} in imaginary part of impedance C'' vs.

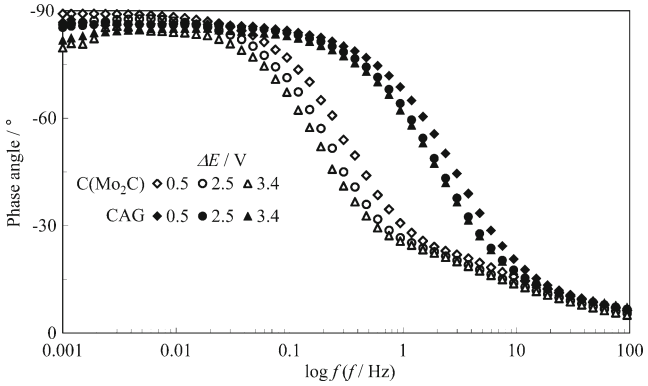

Fig. 4 Phase angle vs. *ac* frequency plots at cell potentials ΔE of 0.5, 2.5 and 3.4 V

ac frequency plots [23, 24]. C'' was calculated from Nyquist plot data according to the following equation [25]:

$$C''(\omega) = \frac{Z'(\omega)}{\omega |Z(\omega)|^2} \tag{3}$$

where $\omega = 2\pi f$.

Time constants were calculated using relation 4:

$$\tau_R = \frac{1}{2\pi f_{max}}. \tag{4}$$

The time constant values obtained for CAG-based system (given in Fig. 5) were almost two times shorter, being as short as 0.05 s, compared to the ones for $C(Mo_2C)$-based system. Time constant values somewhat increase with the higher ΔE applied for both systems studied.

The maximal energy density E_{max} (in watt-hours per kilogram) and power density P_{max} (in kilowatts per kilogram) values [25–29] were calculated using relations 5 and 6:

$$E_{max} = \frac{C_s\, S_{el}\, \Delta E^2}{2\, m\, 3.6} \tag{5}$$

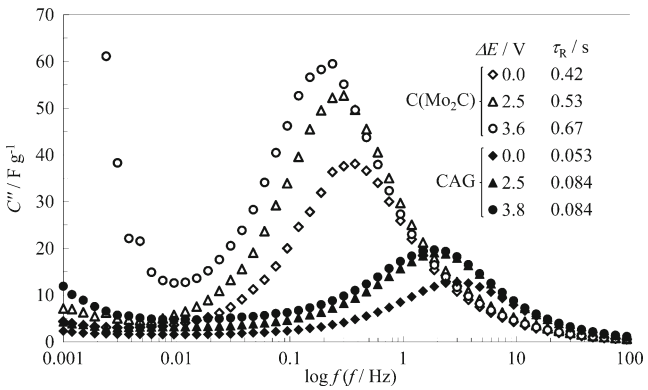

Fig. 5 Imaginary part of capacitance C'' vs. *ac* frequency plots at cell potentials ΔE of 0.0, 2.5 and 3.8 and 0.0, 2.5 and 3.6 for CAG- and $C(Mo_2C)$-based SC test cells, respectively. Characteristic time constants τ_R, calculated for different cell potentials applied, are shown in the figure

$$P_{max} = \frac{\Delta E^2\, S_{el}}{4 R_E\, m} \tag{6}$$

where C_s is low-frequency series capacitance (in farads per square centimetre), S_{el} is the cross-section surface area of electrodes (2 cm^2), m is the mass of two electrodes (in grams) and R_E is high-frequency series resistance (in ohms times square centimetre), obtained from impedance data at very high *ac* frequency (3.6 comes from conversion of time and mass units). For a better comparison, the volumetric energy and power densities ($E_{max,V}$ and $P_{max,V}$) were calculated as well. The calculated data for both systems studied are given in Table 2. Higher energy density values (maximum of 63 Wh kg^{-1} or 34 Wh dm^{-3} at ΔE=3.6 V) were obtained for the $C(Mo_2C)$-based system as the equilibrium capacitance was approximately two times higher. Due to the smaller R_E values for the CAG-based system, very high P_{max} values were calculated at ΔE=3.8 V (757 kW kg^{-1} or 314 kW dm^{-3}). There is a small contribution of faradaic current at the highest ΔE applied (3.6 and 3.8 V for $C(Mo_2C)$- and CAG-based systems, respectively) to the energy density values calculated, which is why the values in Table 2 are given also at lower ΔE, where there are no faradaic processes.

Conclusions

Non-aqueous electrolyte-based supercapacitor test cells were assembled and their electrochemical behaviour was compared on the basis of the different carbon electrode materials used. It was found that the CAG, synthesised by pyrolysis of methylresorcinol and formaldehyde derived organic aerogel, demonstrated nearly ideally capacitive behaviour at high ΔE applied ($\Delta E \leq 3.8$ V), and despite the moderate capacitance values obtained (~55 F g^{-1}) due to high degree of mesoporosity in the material, very high power density values (up to 757 kW kg^{-1}) and moderate energy density values were calculated (up to 32 Wh kg^{-1}). The mainly microporous high surface area carbon powder $C(Mo_2C)$, synthesised from molybdenum carbide by high temperature chlorination method, exhibited nearly ideal polarizability at slightly lower cell potentials ($\Delta E \leq 3.6$ V), but

Table 2 Maximal energy and power density values for systems under study

Carbon	ΔE/V	E_{max}/ Wh kg^{-1}	$E_{max,V}$/ Wh dm^{-3}	P_{max}/ kW kg^{-1}	$P_{max,V}$/ kW dm^{-3}
CAG	3.6	26	11	666	278
	3.8	32	13	757	314
$C(Mo_2C)$	3.4	54	30	305	167
	3.6	63	34	322	176

gravimetric capacitance values and also energy density values were much higher (~125 Fg^{-1} and up to 63 Wh kg^{-1}, respectively). The high-frequency series resistance values were slightly higher for the C(Mo_2C)-based system, and in combination with the lower applicable cell potential, the maximal power density values calculated (up to 322 kW kg^{-1}) were half the values for CAG-based supercapacitor test cells.

In conclusion, the tested carbon materials are well suited for the application in non-aqueous supercapacitors with high specific performance. Long-lasting constant current charge/discharge tests of the studied systems are under progress.

Acknowledgements This work has been partially supported by Estonian Science Foundation Grant No. 8172, Estonian Ministry of Education and Research (project SF0180002s08) and by graduate school 'Functional materials and processes' receiving funding from the European Social Fund under project 1.2.0401.09-0079 in Estonia. Prof. Kalle Kirsimäe and Mr. Jaan Aruväli from the Institute of Ecology and Geography and Mrs. Heisi Kurig from the Institute of Chemistry at the University of Tartu are thanked for the help with XRD and adsorption studies of carbon samples.

References

1. Simon P, Gogotsi Y (2008) Nat Mater 7:845–854
2. Lin R, Taberna PL, Chmiola J, Guay D, Gogotsi Y, Simon P (2009) J Electrochem Soc 156:A7–A12
3. Conway BE (1999) Electrochemical supercapacitors: scientific fundamentals and technological applications. Kluwer Academic, New York
4. Miller JR, Simon P (2008) Science 321:651–652
5. Lust E, Jänes A, Arulepp M (2004) J Solid State Electrochem 8:488–496
6. Eikerling M, Kornyshev A, Lust E (2005) J Electrochem Soc 152: E24–E33
7. Frackowiak E, Béguin F (2001) Carbon 39:937–950
8. Pandolfo AG, Hollenkamp AF (2006) J Power Sources 157:11–27
9. Singhal S, Kendall K (2003) High temperature solid oxide fuel cells: fundamentals, design and applications. Elsevier, Oxford
10. Peled E (1983) Ambient temperature lithium batteries. In: Gabano JP (ed) Lithium batteries. Oxford University Press, London
11. Mayer ST, Pekala RW, Kaschmitter JL (1993) J Electrochem Soc 140:446–451
12. Pekala RW, Farmer JC, Alviso CT, Tran TD, Mayer ST, Miller JM, Dunn B (1998) J Non-Cryst Solids 225:74–80
13. Liu X, Juan L, Zhan L, Tang L, Wang Y, Qiao W, Liang X, Ling L (2010) J Electroanal Chem 642:75–81
14. Lust E, Jänes A, Arulepp M (2004) J Electroanal Chem 562:33–42
15. Chmiola J, Dash R, Yushin G, Gogotsi Y (2006) J Power Sources 158:765–772
16. Pérez-Caballero F, Peikolainen A-L, Koel M, Herbert M, Galindo A, Montilla F (2008) Open Pet Eng J 1:42–46
17. Jänes A, Thomberg T, Kurig H, Lust E (2009) Carbon 47:23–29
18. Gregg SJ, Sing KSW (1982) Adsorption. Surface area and porosity. Academic, London
19. ISO-15901-3:2007. Pore size distribution and porosity of solid materials by mercury porosimetry and gas adsorption—part 3: analysis of micropores by gas adsorption
20. Li J, Wang X, Huang Q, Gamboa S, Sebastian PJ (2006) J Power Sources 158:784–788
21. Wu D, Fu R, Yu Z (2005) J Appl Polym Sci 96:1429–1435
22. Lust E, Nurk G, Jänes A, Arulepp M, Permann L, Nigu P, Möller P (2002) Condens Matter Phys 5:307–328
23. Thomberg T, Jänes A, Lust E (2009) J Electroanal Chem 630:55–62
24. Tõnurist K, Jänes A, Thomberg T, Kurig H, Lust E (2009) J Electrochem Soc 156:A334–A342
25. Taberna PL, Simon P, Fauvarque JF (2003) J Electrochem Soc 150:A292–A300
26. Burke AF (2000) J Power Sources 91:37–50
27. Arulepp M, Leis J, Lätt M, Miller F, Rumma K, Lust E, Burke AF (2006) J Power Sources 162:1460–1466
28. Arulepp M, Permann L, Leis J, Perkson A, Rumma K, Jänes A, Lust E (2004) J Power Sources 133:320–328
29. Zhao S, Wu F, Yang L, Gao L, Burke AF (2010) Electrochem Commun 12:242–245